Highlights

- Negligible overpotentials and low Tafel slopes
- Rh spillover effect
- High stability towards hydrogen evolution thanks to the MoS_2 coating
- Extremely high poisoning tolerance for PtRh during MOR
- Very low onset potential towards MOR displayed by PtRh/MoS_2

Figure

	Pt wt. %	*Tafel slope [mV/dec]*	*Overpotential [V]*	*Ref.*
NiPt-Ni_2Pt	**77-62**	**146 - 134**	**--**	37
AuPt	**50**	**34**	**<0.01**	38
MoS_2/RGO	**-**	**41**	**>0.1**	39
MoS_2	**-**	**94**	**>0.2**	34
$NiSMoS_2G$	**-**	**~40**	**~0.08**	34
fct-FePt	**>63**	**--**	**>0**	40
Pd/Pt	**~49**	**Volmer-Heyrovsky mechanism**	**0.05**	11
Cu/Pt	**~35**	**Volmer-Heyrovsky mechanism**	**Negligible**	8
Pt@Te-rGO/polyimide	**-**	**55**	**0.04**	41
Pt/PtO_2	**-**	**31**	**Negligible**	35
PtRh	**73**	**18**	**Negligible**	**This work**
PtRh-MoS_2	**47**	**32.7**	**Negligible**	**This work**

Table 1 Comparison of HER performances between our samples and some of the most performing nano-electrocatalysts reported in literature.

catalyst	*Potentials (V)*				*Ref.*
	onset	***anodic peak***	***I_f/I_b ratio***	***Reference electrode***	
$Pt_{52}Ru_{48}/C$	**0.02**	**0.62**	**2.3**	**SCE**	**44**
$Pt/Ru–RuO_2$	**0.533**	**0.7***	**1.9**	**Ag/AgCl**	**45**
$Pt\text{-}MoS_2$	**0.17**	**0.53**	**1.44**	**SCE**	**24**
Pt-graphene	**0.25**	**0.53**	**1.18**	**SCE**	**24**
Commercial Pt/C	**0.35**	**0.55***	**0.95**	**SCE**	**24**
$Pt_{32}Cu_{68}$	**0.2***	**0.68***	**1.34**	**SCE**	**10**
Ni_{50}/Pt/Porous Carbon Nanofibers	**0.43**	**0.69***	**1.1***	**Ag/AgCl**	**46**
Ni-C-Pt	**0.25***	**0.65**	**1.12**	**SCE**	**47**
PtRu nanodendrites	**0.4***	**0.62**	**1.66**	**Ag/AgCl**	**14**
PtRh	**0.18**	**0.24**	**4.66**	**SCE**	**This work**
$PtRh\text{-}MoS_2$	**0.07**	**0.3**	**2.37**	**SCE**	**This work**

*values extrapolated from the Cyclic voltammograms

Table 2 Comparison of MOR performances between our samples and Pt based nano-electrocatalysts reported in literature.

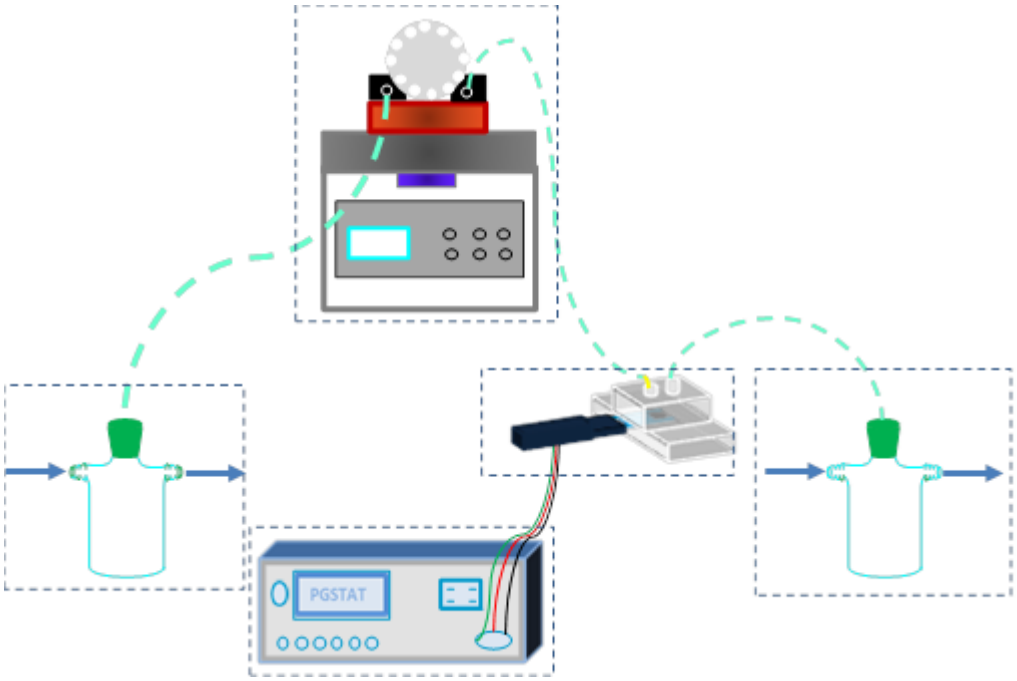

Figure 1 Experimental apparatus for HER tests in a continuous electrolyte flow system.

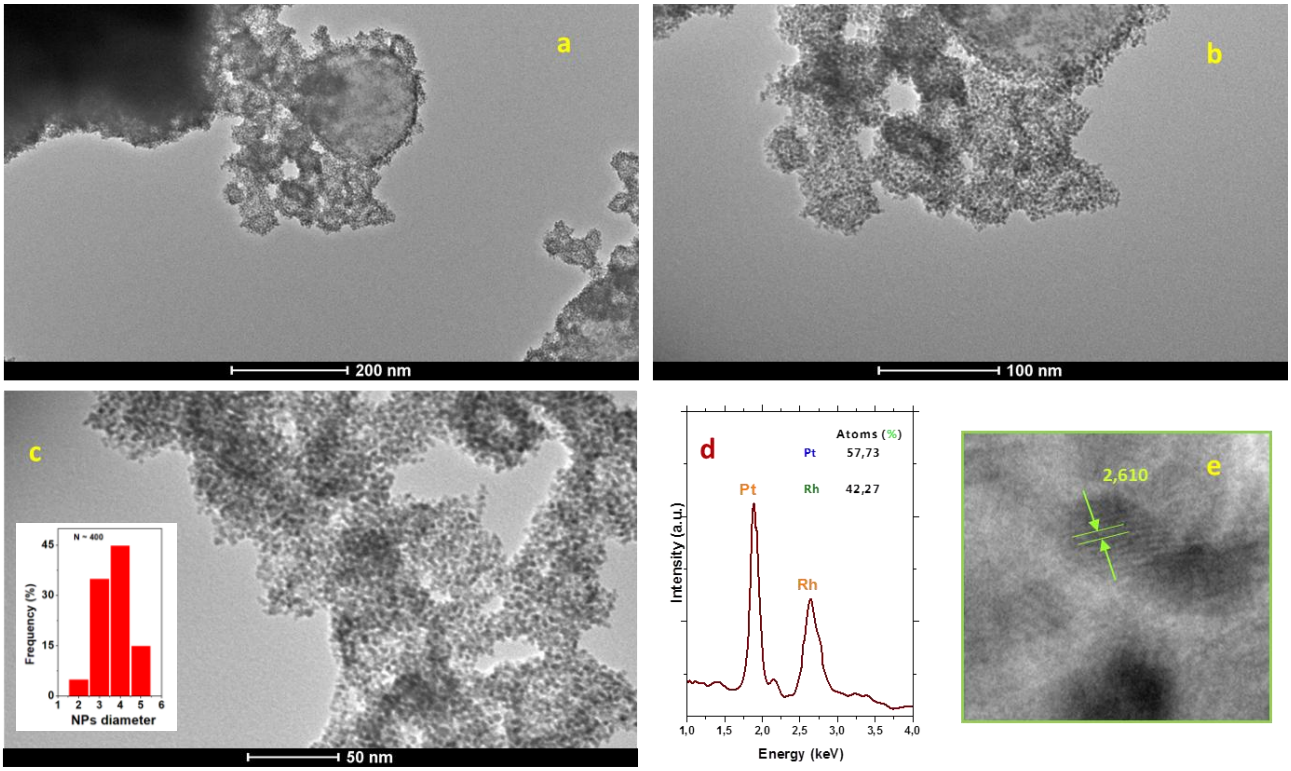

Figure 2 TEM images of PtRh nanoparticles at different magnifications (a,b,c), size distribution histogram in the insert. In addition, EDS spectrum of PtRh is reported (d) together with a high resolution TEM image showing a d spacing of 2.610 Å (e).

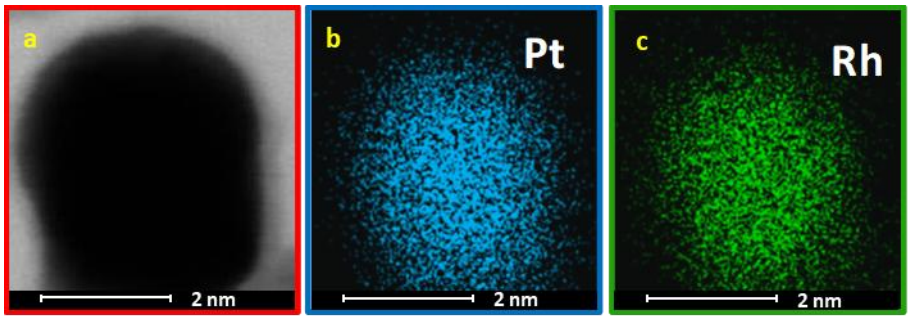

Figure 3 FESEM image of PtRh (a) and EDX maps of platinum and rhodium (b,c).

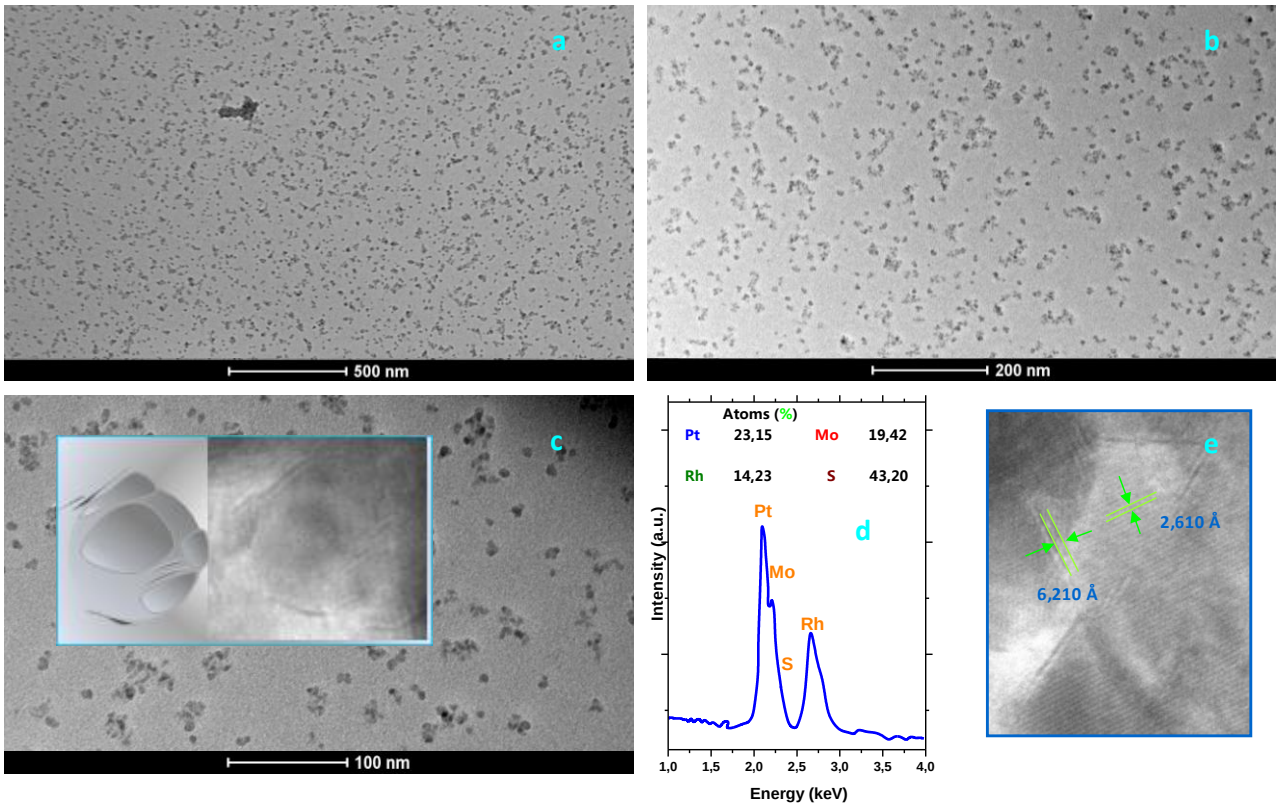

Figure 4 TEM images of PtRh-MoS_2 nanostructures at different magnifications (a,b,c); MoS_2 nanosheets on PtRh nanoparticles (insert in c). EDS spectrum of PtRh-MoS_2 is reported (d); high resolution TEM image showing the interplanar spacings of PtRh alloy and MoS_2 nanosheets (e).

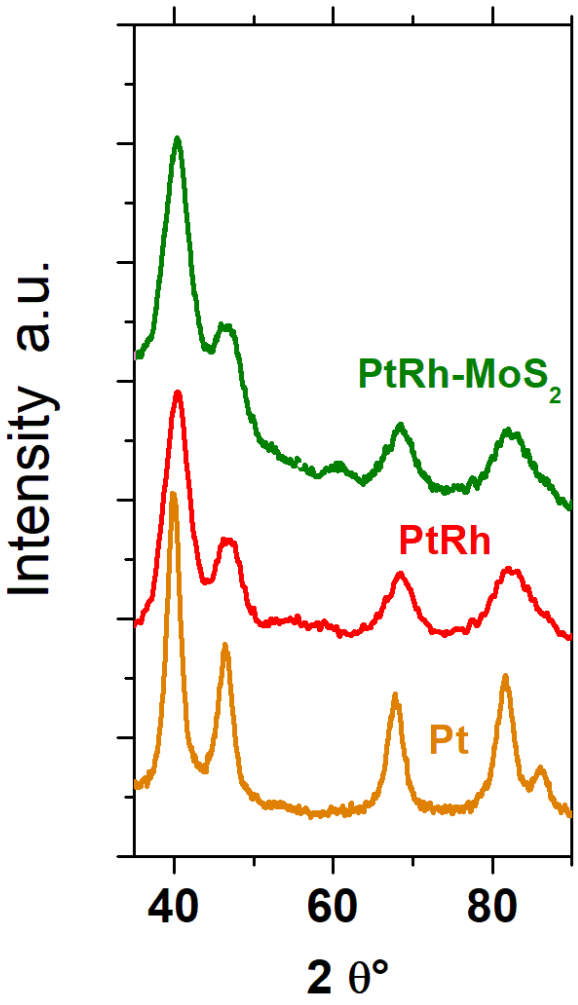

Figure 5 X-ray diffraction patterns of Pt, PtRh and PtRh-MoS_2.

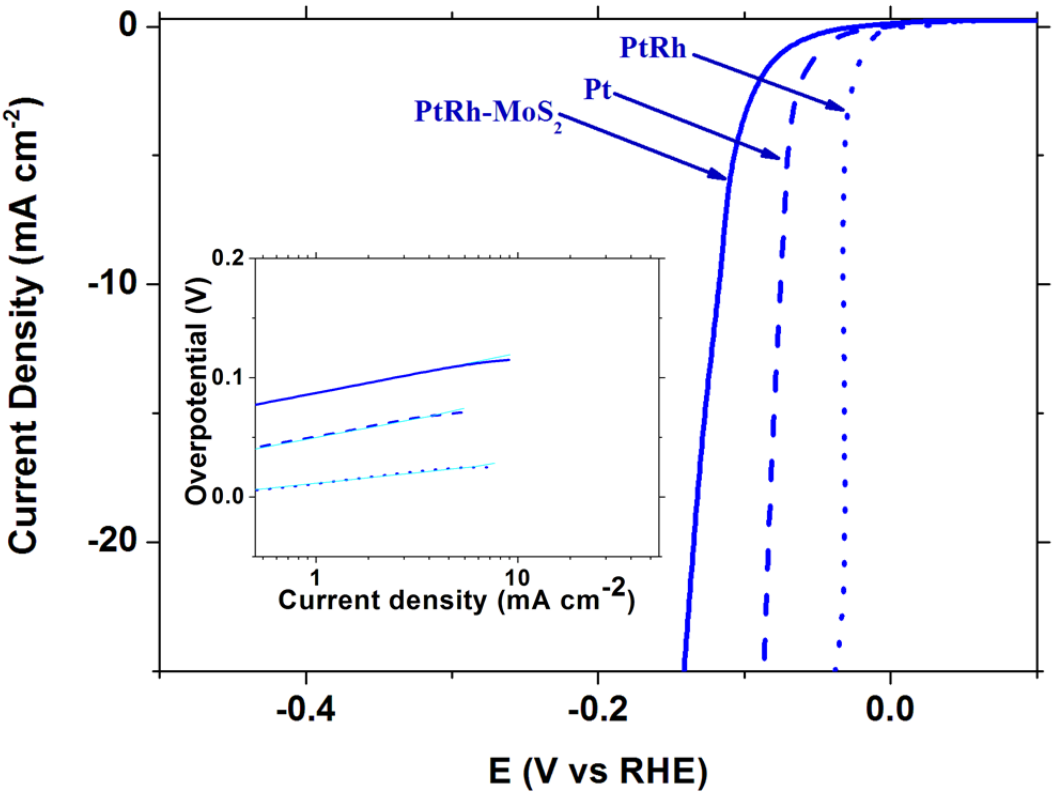

Figure 6 Polarization curves at 20 mV/sec of Pt, PtRh and PtRh-MoS_2 nano-electrocatalysts obtained with a continuous electrolyte flow system. In the insert, Tafel plots for Pt, PtRh and PtRh-MoS_2 obtained with the same system.

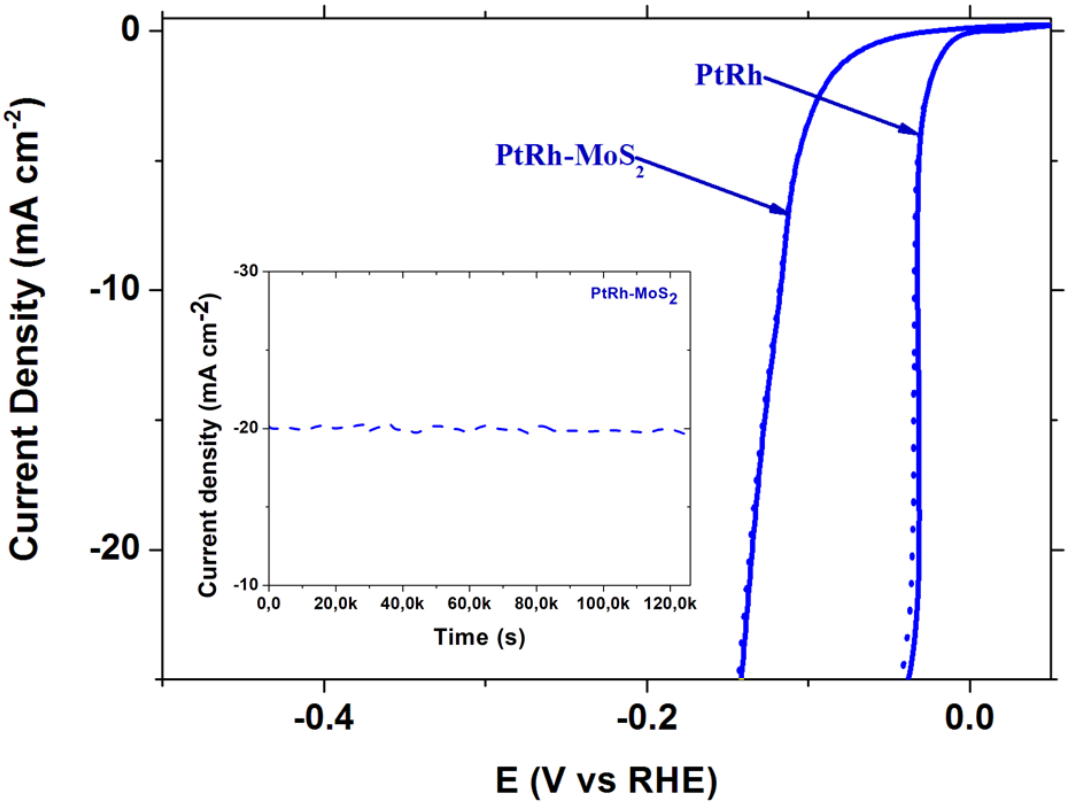

Figure 7 Stability tests: cycling voltammetry before and after 2000 cycles for PtRh and PtRh-MoS_2. In the insert, current density –time curve for PtRh-MoS_2 at -0.13 V.

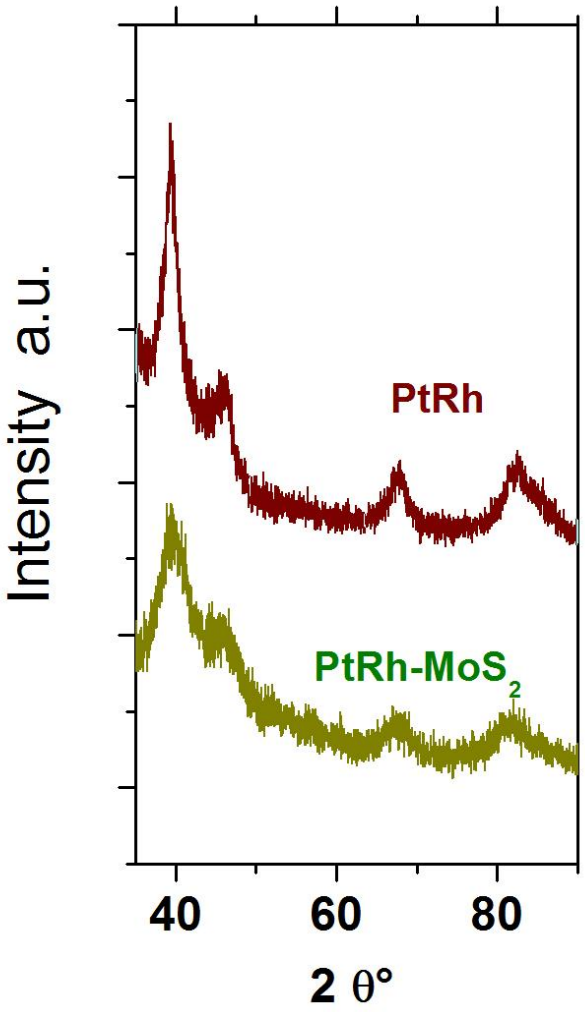

Figure 8 X-ray diffraction patterns of PtRh and PtRh-MoS_2 after electrochemical tests.

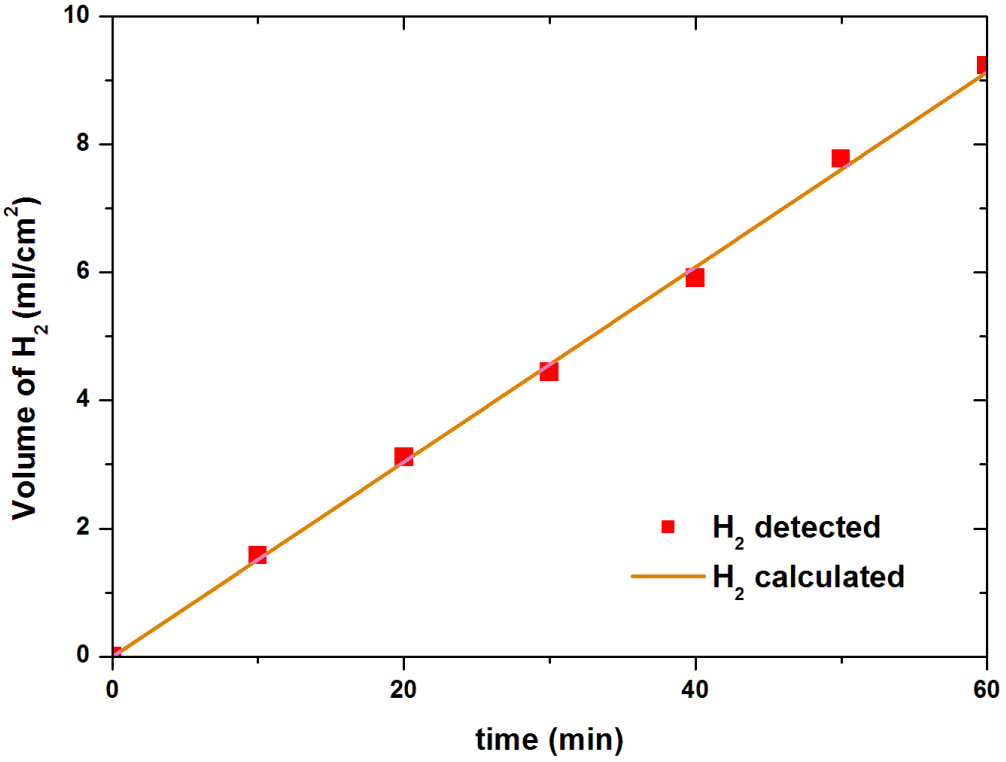

Figure 9 Hydrogen produced practically in red and theoretically in orange. The volume of hydrogen was calculated and detected on PtRh-MoS_2 electrode in 1M H_2SO_4 at -0.13 V.

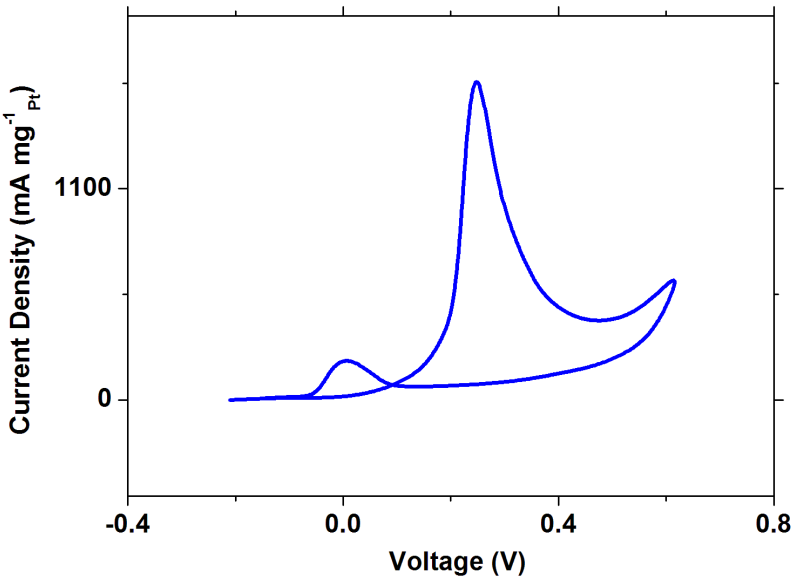

Figure 10 Cyclic voltammogram for methanol oxidation over PtRh sample in a 0.5M H_2SO_4 and 2M CH_3OH solution at a scan rate of 20 mV/s.

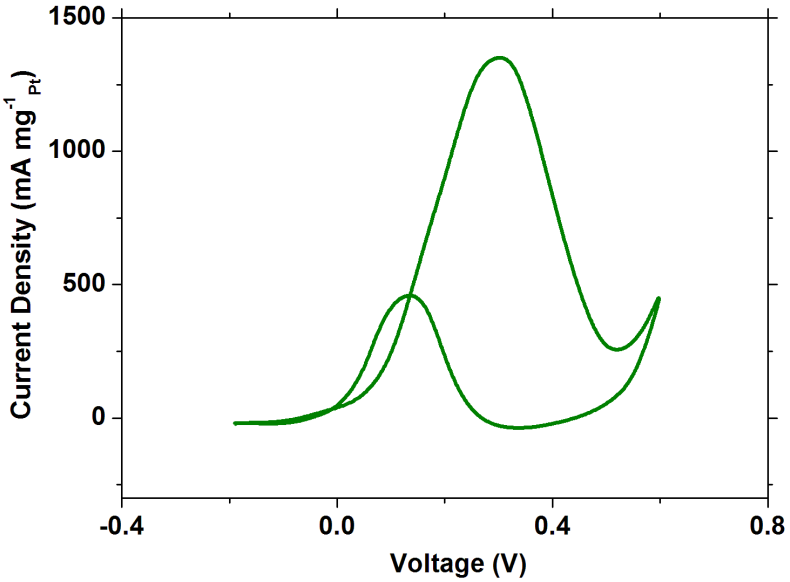

Figure 11 Cyclic voltammogram for methanol oxidation over PtRh-MoS_2 sample in a 0.5M H_2SO_4 and 2M CH_3OH solution at a scan rate of 20 mV/s.

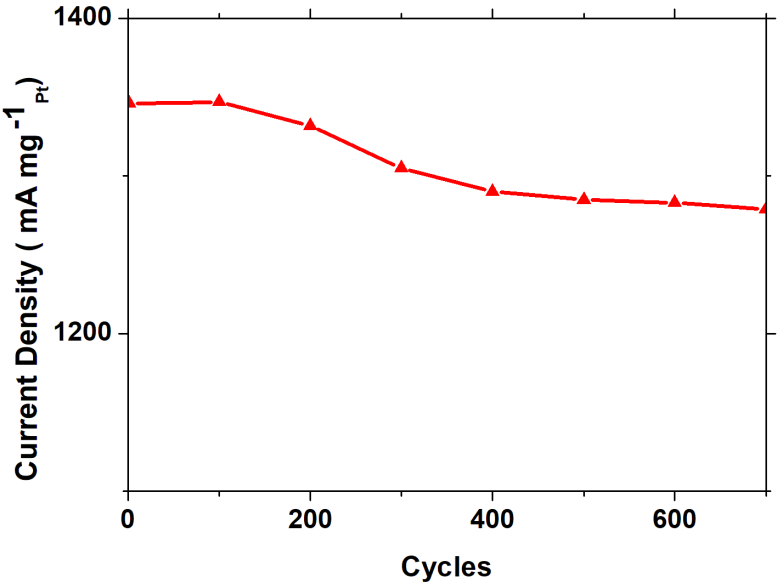

Figure 12 Anodic peak currents in 0.5M H_2SO_4 and 2M CH_3OH solution at different scan cycles for PtRh-MoS_2 sample.

Supporting Info

PtRh and PtRh/MoS_2 nano-electrocatalysts for methanol oxidation and hydrogen evolution reactions

Maria Sarno, Eleonora Ponticorvo, Davide Scarpa

Department of Industrial Engineering and NANO_MATES Research Centre,

University of Salerno, via Giovanni Paolo II, 132 - 84084 Fisciano (SA), Italy

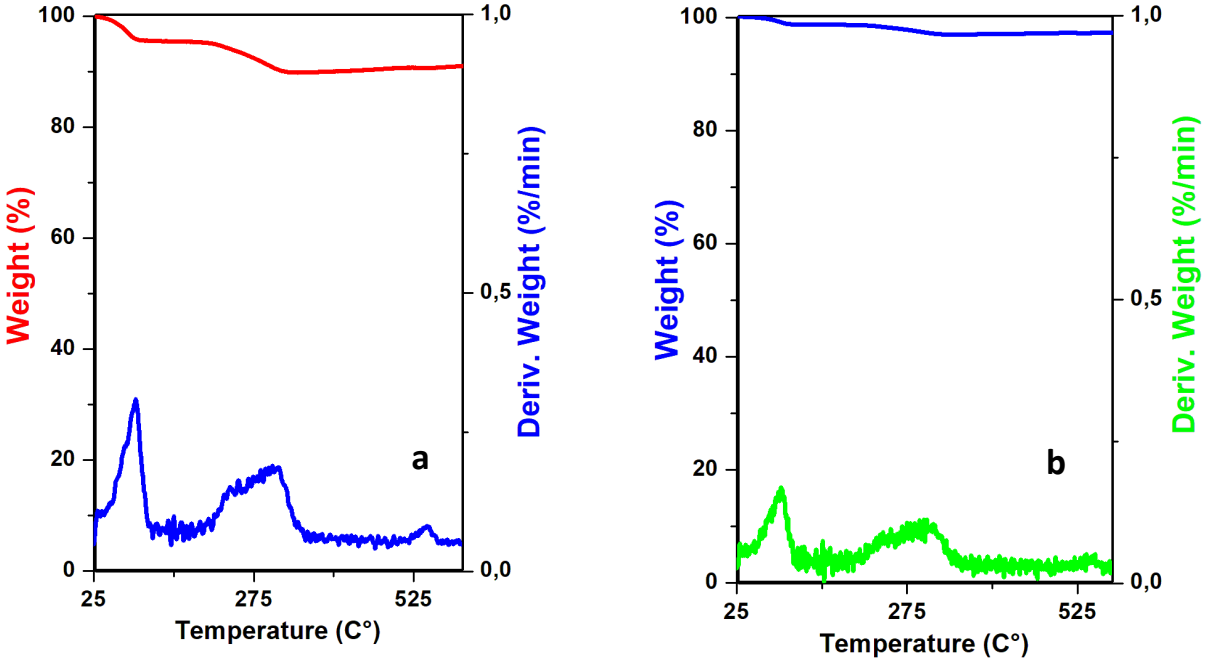

Figure S1. TG-DTG of PtRh as synthesized (a). TG-DTG of PtRh sample after a thermal treatment under air flow, from room temperature up to 150 °C at 10 K/min for 8 h (b).

PtRh and PtRh/MoS_2 nano-electrocatalysts for methanol oxidation and hydrogen evolution reactions

Maria Sarno, Eleonora Ponticorvo, Davide Scarpa

Department of Industrial Engineering and NANO_MATES Research Centre,

University of Salerno, via Giovanni Paolo II, 132 - 84084 Fisciano (SA), Italy

ABSTRACT

A synthesis of PtRh and PtRh covered with MoS_2 nanoelectrocatalysts obtained by means of a scalable, economic, wet chemistry approach is proposed. The synthesized nanocatalysts were broadly characterized: XRD, SEM and TEM images and EDX maps showed the formation of bimetallic PtRh alloy nanoparticles, which in the second sample were covered with MoS_2 nanosheets.

Firstly, the electrocatalytic activity of the synthesized materials was tested towards hydrogen evolution reaction (HER), showing excellent properties: negligible overpotentials and very small Tafel slopes (18 mV/decade and 32.7 mV/decade for PtRh and PtRh-MoS), respectively. The samples exhibited also high stability over time towards HER, especially PtRh/MoS_2. Secondly, the catalysts were tested towards methanol oxidation reaction (MOR), showing low onset potentials (0.18 V for PtRh and 0.07 V for PtRh/MoS_2) and very high *If/Ib* ratio (4.66 for PtRh and 2.37 PtRh/MoS_2). The results obtained in this work evidence the outstanding performances of the synthesized nano-electrocatalysts.

Keywords: PtRh and PtRh/MoS_2 nano-electrocatalyst, methanol oxidation reaction, hydrogen evolution reaction, high hydrogen production rate

*Corresponding authors: Tel.: +39 089 963460; fax: +39 089 964057; E-mail address: msarno@unisa.it (M. Sarno).

1. Introduction

In recent years, hydrogen has been regarded as the best alternative to fossil fuels [1,2]. This promising energy carrier can be produced from a wide variety of renewable and non-renewable resources and offers a long list of advantages [1,2]. Water electrolysis can surely achieve the largest pure hydrogen production starting from a readily available, economic and renewable resource. Besides, liquid alcohols, in particular methanol, recently started to be considered as a link between hydrocarbons and hydrogen, owing to their higher energy densities and ease of storing and supply through the current fuel distribution network [3]. Methanol can be either used in direct methanol fuel cells (DMFC) or converted into hydrogen by thermal or electrochemical reforming, in order to be fed to the much more performing proton exchange membrane fuel cells (PEMFC).

Pure platinum has been extensively explored for its outstanding electrocatalytic performance towards a large amount of reactions, such as methanol oxidation reaction (MOR) and hydrogen evolution reaction (HER), which are fundamental in methanol and water electrolysis respectively. Nevertheless, the industrial-scale production and application have been significantly hampered by the high price and scarce availability of this precious metal. Moreover, pure platinum is not highly effective towards MOR due to the production during methanol oxidation of intermediate carbonaceous species (mainly CO), which can significantly reduce the reaction kinetics by poisoning the Pt catalytic surface [4,5,6]. Therefore, to reduce the poisoning, improve the electrocatalytic performance of Pt and minimize the its usage, Pt-based bimetallic nanostructures have attracted increasing interest during the past decade as the best alternative to pure Pt for both HER [7,8] and MOR [9,10]. For instance, Reja Ojani et al. [11] prepared and characterized bi-component PdPt deposited on copper electrode for catalysis of HER in acidic media. The authors

clearly explained the improved HER performances of the PtPd catalyst as a consequence of a synergistic effect occurring between the two metals. A key to further understanding this phenomenon is provided by the “d-band center theory”. According to this theory, the surface metal d-band is involved in the chemical bond with the adsorbate and the position of the d-band center compared to the Fermi level plays a governing role in determining the strength of the metal-adsorbate interaction. Alloying a metal M_1 with another metal M_2 modifies the surface bond lengths M_1-M_1 as a consequence of the introduction in the M_1 lattice of M_2 atoms with a different lattice constant (strain effect) and, at the same time, the presence of M_2 around metal M_1 atoms changes its electronic environment (ligand effect). Both phenomena contribute to modify the d-band width of M_1, therefore causing a shift of the d-band center which results in either a strengthening or a weakening of the M_1-absorbate bond [12,13]. The same effect has been observed on PtRu nanodendrites bimetallic catalysts [14] tested towards methanol oxidation. As mentioned before, an efficient catalyst for MOR must guarantee a high tolerance against the incompletely oxidized species which can be strongly adsorbed on their surfaces and the authors clarified that the strain effect arising from alloying Ru with Pt contribute to weaken the bond between the metal and the adsorbate, improving the catalyst efficiency. Moreover, a bifunctional mechanism, i.e. faster water activation on Ru surface, can also contribute to the improved performance of Pt/Ru catalyst [15]. It is clear, therefore, that nanostructures comprising Pt and a noble metal alloy can achieve enhanced performances for both HER and MOR.

Amongst noble metals, rhodium can be regarded as an excellent material, being at the top of Trasatti’s volcano plot [16] and because of its oxophilic nature which can provide a lower MOR onset potential [17]. Furthermore, the presence of Rh into the Pt lattice may weaken the CO-Pt bond because of the up-shifting of the metal d-band center and the increasing repulsive

interaction, whereas hydroxide species easily adsorbed on this metal can further improve CO tolerance [18].

PtRh as a nanocatalysts for both HER and MOR has been little explored till now. This is probably because of the rhodium price, which has been very changeable over the last years. For instance, in 2003 its value was about $500/oz, but an increase in demand caused a sharp rise in price until 2008, when it almost reached $10,000/oz, whilst a new decrease was registered after that episode [19]. Nowadays, rhodium price is strictly connected to the automobile market, since more than 80% of the whole world supply is requested by the automotive catalyst industry. In fact, rhodium is fundamental in catalytic converters for both gasoline and, especially, diesel engines [20]. Albeit the world rhodium market is still solid as a consequence of the still high demand of the noble metal by automobile industries, in the long run the rise of hybrid and electric vehicles is expected to heavily impact that market, causing, therefore, rhodium price to plummet, which will make this metal more affordable than platinum [21].

Currently, considerable attention has been focused on 2D nanomaterials such as MoS_2, which has been found to be a highly efficient catalyst for HER due to its characteristic graphene-like two-dimensional structure [22,23]. MoS_2 exhibits excellent electrocatalytic activity towards MOR as well, because of its high tolerance toward CO poisoning [24].

Herein, for the first time, a synthesis of PtRh and PtRh covered with MoS_2 nanoelectrocatalysts obtained by means of a scalable, economic, wet chemistry approach is proposed. After being synthesized, the catalysts were characterized and tested for both HER and MOR showing outstanding electrocatalytic performances and remarkable stability over time, likely due to the presence of a MoS_2 coating around the metals.

2. Materials and methods

2.1 PtRh nanostructures and Pt nanoparticles preparation

PtRh nanostructures, in the following named PtRh as synthesized, were obtained in 1-octadecene using 1-2 hexadecanediol as reducing agent and oleylamine and oleic acid as surfactants [25,26,27] by thermal decomposition of platinum(II) acetylacetonate and rhodium(III) nitrate hydrate under N_2 flow. In particular, 0.61659 mmol of $Pt(C_5H_7O_2)_2$ and 0.43265 mmol of $Rh(NO_3)_3{\times}H_2O$ were mixed with 20 mL of 1-octadecene, 10 mmol of 1,2-hexadecanediol, 6 mmol of oleylamine and 6 mmol of oleic acid. Oleylamine was used not only as a surfactant but also as stabilizer and mild reducing agent, being able to donate electrons at high temperatures [28]. With regard to the PtRh synthesis, the mixture was heated to 200 °C for 120 min and then further heated to reflux (~300 °C) for 60 min. Moreover, for comparison, Pt nanoparticles, in the following named Pt NPs as synthesized, were also prepared with the same procedure by using only platinum(II) acetylacetonate as precursor.

2.2 PtRh-MoS_2 nanostructures preparation

PtRh-MoS_2 nanostructures, in the following named PtRh-MoS_2 as synthesized, were prepared using the same method of the previous samples. In detail, in order to perform this last synthesis the following chemicals were used: platinum(II) acetylacetonate (0.61659 mmol), rhodium(III) nitrate hydrate (0.43265 mmol), ammonium tetrathiomolybdate (0.57613 mmol), 1-octadecene (20 mL), 1,2-hexadecanediol (10 mmol), oleic acid (6 mmol) and oleylamine (6 mmol).

2.3 PtRh, Pt NPs and PtRh-MoS_2 post synthesis treatments

The organic chains covering the synthesized samples have the double function of stabilizing and preventing nanostructures aggregation, yet exhibit a resistive behavior. Therefore, in order to reduce the chains amount, the PtRh, Pt and PtRh-MoS_2 nanostructures underwent a thermal

treatment under air flow, from room temperature up to 150 °C at 10 K/min for 8 h, which allowed the reduction of about 70 wt. % of organic chains amount [29], see Figure S1.

2.4 Characterization

Several techniques have been adopted in order to characterize the synthesized samples. Transmission electron microscopy (TEM) was performed with a FEI Tecnai electron microscope operated at 200 KV with a LaB_6 filament as electron source, whilst field emission scanning electron microscopy (FESEM) images were obtained by the use of a LEO 1525 electron microscope. Both the microscopes were equipped with an energy dispersive X-ray (EDX) probe. A Bruker D8 X-ray diffractometer with a monochromatic CuKα radiation was used for measurements of powder diffraction profiles.

Through the use of an Autolab PGSTAT302N potentiostat, the electrochemical performances towards HER were evaluated by linear sweep voltammetry tests in a 1M H_2SO_4 solution, whereas, in order to investigate the electrochemical performances towards MOR, cyclic voltammetry was performed by testing the samples in a 0.5 M H_2SO_4 and 2 M CH_3OH solution.

Before the electrochemical measurements, 8 mg of synthesized sample were dispersed into 160 µl of a 5 wt% Nafion solution, 900 µl of 2-propanol and 100 µL of water in order to obtain a homogeneous suspension which, after a 30 min sonication treatment and subsequent drying in air, was partly deposited dropwise onto a Screen Printed Electrode (SPE) consisting of a carbon working electrode, a platinum counter electrode and a silver reference electrode. Graphite SPEs were chosen owing to their superior characteristics over common carbon electrodes [30].

Furthermore, with a view to simulating a system as close as possible to the industrial one, an experimental configuration with a continuous electrolyte flow was adopted in order to evaluate the samples performances towards HER. As shown in Figure 1, the apparatus consists of an electrolytic cell containing the sample deposited on an SPE and connected to the potentiostat

through a cable system. The inlet and outlet electrolyte flow is regulated by a variable-flow peristaltic pump. This new system allows to reduce the process energy consumption by lowering the mass transfer resistance due to the hydrogen bubbles both released in solution and deposited onto the electrode. Lastly, in order to evaluate the hydrogen amount produced in the electrolytic cell, quantities at different times were withdrawn from the electrolytic solution and examined through gas chromatography-mass spectrometry analysis, by the means of a Thermo Scientific FOCUS GC-ISQ Single Quadrupole MS. After obtaining the calibration curve from the analysis of known quantities of hydrogen, the amount of gas produced was evaluated from the areas under the peaks of interest and compared with the theoretical amount in order to calculate the hydrogen production efficiency.

3. Results and discussion

3.1 Morphological characterization

The morphological and structural characteristics of the samples were determined by transmission electron microscopy (TEM) and field emission scanning electron microscopy (FESEM) analysis. Both the microscopes were equipped with an EDX probe. With regard to the PtRh nanostructures, TEM images at different magnifications (scale bars: 200, 100 and 50 nm), Figure 2 a,b,c, show the formation of nanoparticles with an average diameter of about 3-4 nm (see also the size distribution histogram in the inset, about 400 nanoparticles were considered to obtain their size distribution histograms). The result of the EDS analysis is also reported, displaying a Pt/Rh atomic ratio in line with the percentages of Pt and Rh in the precursors chosen for the synthesis, whilst the high resolution TEM image shows an interplanar spacing of 2.610 Å which does not match the ones of Pt and Rh alone, showing the presence of a PtRh alloy (Figure 2 d,e). In addition, in Figure 3 the high resolution FESEM image and the corresponding EDX maps for each metal reveal, being

superimposable on each other, that platinum and rhodium are homogeneously distributed in the sample, therefore confirming the formation of a binary alloy.

With reference to PtRh-MoS_2, TEM images at different magnifications (scale bars: 500, 200 and 100 nm) were also collected, showing that such nanocatalyst is constituted of nanostructures well separated from each other comprising PtRh nanoparticles covered with few MoS_2 nanosheets (Figure 4 a,b,c and insert). Even in this case, the EDS analysis shows an atomic ratio in line with the percentages of the elements in the precursors (Figure 4 d), showing the formation of a PtRh alloy, whose typical (111) crystalline plane is distinctly highlighted in the high resolution TEM image (Figure 4 e) with the corresponding interplanar distance of 2.610 Å, together with the MoS_2 nanosheets interplanar spacing of 6.210 Å [31].

3.2 X-ray diffraction analysis

Figure 5 shows the X-ray patterns of Pt, PtRh and PtRh-MoS_2 nanostructures. As for the Pt nanoparticles, the diffraction peaks are coincident with the pure fcc Pt characteristic peaks (JCPDS: 04-0802) at 2θ: 39.79°, 46.24°, 67.45°, 81.29° and 85,70° [32]. Regarding PtRh, the X-ray diffraction pattern clearly evidences a slight up-shift of the peaks of pure Pt owing to the alloy formation. This phenomenon is due to the lattice contraction caused by the incorporation of Rh into the Pt lattice, which subsequently implies the purity of the formed PtRh alloy without undesired phases. Furthermore, the diffraction pattern of PtRh-MoS_2 also exhibits peaks slightly shifted to intermediate 2θ values with respect to the ones of pure metals, which proves again the existence of a PtRh alloy. These peaks cover the MoS_2 spectrum and lie between both of pure fcc Pt (JCPDS: 04-0802) and pure fcc Rh (JCPDS: 05-0685) at 2θ: 40.49°, 46.9°, 68.67° and 82.26°. Also, in the same pattern, an weak additional peak at 2θ ~ 60° could be recognized, which can be ascribed to the presence of MoS_2 nanosheets in the PtRh-MoS_2 nanostructure [33].

3.3 Electrochemical Hydrogen Evolution Reaction

Firstly, the electrocatalytic activity, towards HER of our nanomaterials deposited on a SPE, both adopting a static 1 M H_2SO_4 solution and using the aforementioned experimental configuration with a continuous electrolyte flow, was investigated. Polarization curves for PtRh and PtRh-MoS_2 were reported in Figure 6, together with the Pt nanoparticles polarization curve for comparison. Our nanostructures exhibit, especially in the electrolyte flow configuration, negligible overpotentials, beyond which the catodic current density, calculated as measured current divided by the available surface of the sample, increases very quickly under more negative WE potentials. In addition to that, these values are comparable to the Pt NPs overpotential. Furthermore, starting from the polarization curves, the corresponding Tafel curves were constructed. The linear portions of these curves were fitted by the Tafel equation [34,35] leading to very small Tafel slope values.

More specifically, overpotentials and Tafel slopes for PtRh and PtRh-MoS_2 are reported in Table 1, row eleven and twelve, respectively. Since polarization curves were iR corrected, Tafel slopes for the static and the electrolyte flow system are very similar. Therefore, only Tafel slopes obtained using the latter system were reported, each of them indicating a high reaction rate (18 and 32.7 mV/decade for PtRh and PtRh-MoS_2 respectively), whereas overpotentials measured on PtRh and PtRh-MoS_2 in the flow configuration are negligible [36]. Literature values, chosen among the most performing nano-electrocatalysts thus far studied, were also reported in the same Table [8,11,34,35,37–41]. The comparison of electrocatalytic performances evidences that our samples are extremely promising: both PtRh and PtRh-MoS_2 show an excellent behavior towards HER, comparable with that of pure platinum and other performing materials. It is well established that Pt is the most performing electrocatalyst towards HER. After all, results show that alloying it with Rh, which is placed close to Pt at the summit of Trasatti's volcano plot [16], provides remarkable HER performances with a reduced Pt amount. In particular, the Tafel slope observed for PtRh is lower than the typical value for a Volmer-Tafel mechanism, that is 30 mV/decade, suggesting a different catalytic mechanism in the presence of Rh. On the other hand, a spillover effect, a phenomenon in which an adsorbed H atom on Rh may easily migrate on other sites, can be the reason of this behavior [42]. Moreover, MoS_2, which probably works as catalyst itself because of its abundant exposed edges, acts as a noble metal electron enhancer and as an additional surface for spillover, exercising simultaneously a stabilizing effect.

In fact, the stability over time of the synthesized electrocatalysts was also tested (see Figure 7). The continuous cycling voltammogram evidences a high durability, especially for PtRh-MoS_2. The initial polarization curve was compared with the curve obtained after 2000 cycles and the two curves appear almost overlapped, showing a high stability of the sample likely due to the MoS_2 coating. On the other hand, the X-ray diffraction analysis after cycles shows a well conserved

structure for both the nanocatalysts [43], as can be seen from Figure 8. Overall, the results indicate that PtRh-MoS_2 nanomaterial, constituted of Pt/Rh nanoparticles stabilized by the MoS_2 nanosheets laying on their surface, can be a useful, stable and efficient alternative HER catalyst. Furthermore, the amount of hydrogen produced using PtRh-MoS_2 nanocatalysts was evaluated. The volumes of hydrogen produced at several times, evaluated from the equation 2nF/Q (n moles of H_2 produced, F Faraday constant and Q cell charge amount in Coulomb), at a voltage of -0.13 V, were plotted in Figure 9 (orange line). They were also analyzed through gas chromatography-mass spectrometry and the quantities of hydrogen detected, red points, are in good agreement with theoretical data obtained when considering the amount of charges passing through the system, which proves a high hydrogen production efficiency.

3.4 Electrochemical Methanol Oxidation Reaction

Secondly, the electrocatalytic activity towards MOR of our nanomaterials deposited on a SPE was tested in a 0.5 M H_2SO_4 and 2 M CH_3OH static solution. Cyclic voltammograms for PtRh and PtRh-MoS_2 at 20 mV/s are shown in Figures 10 and 11 and the results obtained are summarized in Table 2. In the same table the literature values of the most performing nano-electrocatalysts synthesized thus far [10,14,24,44-47] were also collected.

Onset potentials measured on PtRh and PtRh-MoS_2 are found to be 0.18 and 0.07 V respectively, which indicates a low energy required for the redox reactions to occur. This is likely due to the oxophilic nature of Rh [17]. In particular, PtRh-MoS_2 exhibits one of the lowest onset potentials among the ones reported and the main reason for the improved performance can be due to the presence of the MoS_2 coating surrounding the nanoparticles, which further improves catalytic activity towards CO oxidation and CO tolerance [24]. The excellent electrocatalytic performances of our samples were then confirmed by looking at the *If/Ib* ratio (where *If* is the forward peak current density and *Ib* is the backward peak current density) which for PtRh and PtRh-MoS_2 is very

high: 4.66 and 2.37 V respectively. This ratio is often used to quantify the catalyst tolerance against the incompletely oxidized species which are accumulated on its surface [4,48] and its value for PtRh is the highest found in literature thus far, showing the extremely high tolerance of our sample against poisoning, and suggesting not to ignore Rh as a key component of MOR nanocatalysts. Indeed, it is highly likely that the introduction of Rh into the Pt lattice can weaken the Pt-CO bond, by down-shifting the d-band center of Pt, and increase the CO oxidation rate thanks to its oxophilicity [12,13,17,18]. Moreover, PtRh-MoS_2 shows an excellent combination of properties, including a very high specific hydrogen production with respect to the content of the two noble metals.

The anodic peak currents at different cycles for PtRh-MoS_2 are shown in Fig. 12. Current density reached the maximum value after the first 100 cycles, and then it decreases gradually, showing a good stability, also if compared with other papers [49].

4. Conclusions

In summary, PtRh and PtRh-MoS_2 nano-electrocatalysts, through a scalable, economic, one-step synthesis, were successfully prepared. Analyses of XRD results, SEM and TEM images and EDX maps revealed the formation of a bimetallic PtRh alloy nanoparticles with average diameters up to 3-4 nm. In the PtRh-MoS_2 sample, the PtRh alloy nanoparticles are covered with few MoS_2 nanosheets, which thanks to their reduced dimensions expose high edges surface.

PtRh shows excellent HER activity, comparable to the one of pure Pt, and this can be regarded as a consequence of the synergistic effect deriving from alloying the two metals, both of which located at the summit of volcano plot. In particular, the PtRh Tafel slope value suggests a different catalytic mechanism, i.e. hydrogen production takes advantage of a spillover effect. Moreover, MoS_2 nanosheets, probably working as catalyst itself with their abundant exposed edges, acts as a

noble metal electron enhancer, as an additional surface for spillover and possesses a stabilizing effect.

The synthesized nano-electrocatalysts were also tested towards MOR, and PtRh shows the stronger poisoning resistance ever reported in literature. This may be due to the introduction of Rh into the Pt lattice, which weakens the Pt-CO interaction and favors the oxidation of the adsorbed poisons. Moreover, PtRh-MoS_2 shows an excellent combination of properties, including an even lower onset potential than PtRh and a very high specific hydrogen production with respect to the content of the two noble metals.

References

[1]. I. Dincer, C. Acar, Review and evaluation of hydrogen production methods for better sustainability, Int. J. Hydrog. Energy 40 (2015) 11094–11111.

[2]. R.D. Cortright, R.R. Davda, J.A. Dumesic, Hydrogen from catalytic reforming of biomass-derived hydrocarbons in liquid water, Nature 418 (2002) 964–967.

[3]. C.R. Cloutier, D.P. Wilkinson, Electrolytic production of hydrogen from aqueous acidic methanol solutions, Int. J. Hydrog. Energy 35 (2010) 3967–3984.

[4]. D. Liu, L. Li, T. You, Superior catalytic performances of platinum nanoparticles loaded nitrogen-doped graphene toward methanol oxidation and hydrogen evolution reaction, J. Colloid Interface Sci. 487 (2017) 330–335.

[5]. X. Zhao, M. Yin, L. Ma, L. Liang, C. Liu, J. Liao, T. Lu, W. Xing, Recent advances in catalysts for direct methanol fuel cells, Energy Environ. Sci. 4 (2011) 2736–2753.

[6]. H. Huang, X. Wang, Recent progress on carbon-based support materials for electrocatalysts of direct methanol fuel cells, J. Mater. Chem. A 2 (2014) 6266–6291.

[7]. X. Weng, Y. Liu, K.K. Wang, J.J. Feng, J. Yuan, A.J. Wang, Q.Q. Xu, Single-step aqueous synthesis of AuPt alloy nanodendrites with superior electrocatalytic activity for oxygen reduction and hydrogen evolution reaction, Int. J. Hydrog. Energy 41 (2016) 18193–18202.

[8]. J.B. Raoof, R. Ojani, S.A. Esfeden, S.R. Nadimi, Fabrication of bimetallic Cu/Pt nanoparticles modified glassy carbon electrode and its catalytic activity toward hydrogen evolution reaction, Int. J. Hydrog. Energy 35 (2010) 3937–3944.

[9]. Z. Liu, X.Y. Ling, X. Su, J.Y. Lee, Carbon-Supported Pt and PtRu Nanoparticles as Catalysts for a Direct Methanol Fuel Cell, J. Phys. Chem. B 108 (2004) 8234–8240.

[10]. Y. Liao, G. Yu, Y. Zhang, T. Guo, F. Chang, C.J. Zhong, Composition-Tunable PtCu Alloy Nanowires and Electrocatalytic Synergy for Methanol Oxidation Reaction, J. Phys. Chem. C 120 (2016) 10476–10484.

[11]. R. Ojani, J.B. Raoof, E. Hasheminejad, One-step electroless deposition of Pd/Pt bimetallic microstructures by galvanic replacement on copper substrate and investigation of its performance for the hydrogen evolution reaction, Int. J. Hydrog. Energy 38 (2013) 92–99.

[12]. J.R. Kitchin, J.K. Nørskov, M.A. Barteau, J.G. Chen, Modification of the surface electronic and chemical properties of Pt(111) by subsurface 3d transition metals, J. Chem. Phys. 120 (2004) 10240–10246.

[13]. A. Ruban, B. Hammer, P. Stoltze, H.L. Skriver, J.K. Nørskov, Surface electronic structure and reactivity of transition and noble metals, J. Mol. Catal. Chem. 115 (1997) 421–429.

[14]. S. Lu, K. Eid, D. Ge, J. Guo, L. Wang, H. Wang, H. Gu, One-pot synthesis of PtRu nanodendrites as efficient catalysts for methanol oxidation reaction, Nanoscale 9 (2017) 1033–1039.

[15]. P. Waszczuk, A. Wieckowski, P. Zelenay, S. Gottesfeld, C. Coutanceau, J.M. Léger, C. Lamy, Adsorption of CO poison on fuel cell nanoparticle electrodes from methanol solutions: a radioactive labeling study, J. Electroanal. Chem. 511 (2001) 55–64.

[16]. P. Quaino, F. Juarez, E. Santos and W. Schmickler, Volcano plots in hydrogen electrocatalysis - uses and abuses, Beilstein J. Nanotechnol. 5 (2014) 846–854.

[17]. B. Gurau, R. Viswanathan, R. Liu, T.J. Lafrenz, K. L. Ley, E.S. Smotkin, Structural and Electrochemical Characterization of Binary, Ternary, and Quaternary Platinum Alloy Catalysts for Methanol Electro-oxidation, J. Phys. Chem. B 102 (1998) 9997–10003.

[18]. R.A. Van Santen, A. De Koster, T. Koerts, The quantum chemical basis of The Fischer-Tropsch reaction, Catal. Lett. 7 (1990) 1–14.

[19]. One of the Rarest Precious Metals Is on Best Run in a Decade. https://www.bloomberg.com/news/articles/2017-03-07/one-of-the-rarest-precious-metals-is-on-the-best-run-in-a-decade, 2017 (accessed 29 May 2018).

[20]. Annual Integrated Report 2017. http://implats-reports.co.za/reports/pdf/2017/implats-iar-2017.pdf, 2017 (accessed 29 May 2018).

[21]. Copper demand for electric cars to rise nine-fold by 20127: ICA. https://www.reuters.com/article/us-copper-demand-electric-vehicles/copper-demand-for-electric-cars-to-rise-nine-fold-by-2027-ica-idUSKBN1940PC 2017 (accessed 29 May 2018).

[22]. L. Yang, P. Liu, J. Li, B. Xiang, Two-Dimensional Material Molybdenum Disulfides as Electrocatalysts for Hydrogen Evolution, Catalysts 7 (2017) 285–302.

[23]. X. Huang, Z. Zeng, S. Bao, M. Wang, X. Qi, Z. Fan, H. Zhang, Solution-phase epitaxial growth of noble metal nanostructures on dispersible single-layer molybdenum disulfide nanosheets, Nat. Commun. 4 (2013) 1444, 1–8.

[24]. S.H. Patil, B. Anothumakkool, S.D. Sathaye, K.R. Patil, Architecturally designed Pt–MoS_2 and Pt–graphene composites for electrocatalytic methanol oxidation, Phys. Chem. Chem. Phys. 17 (2015) 26101–26110.

[25]. M. Chen, J.P. Liu, S. Sun, One-Step Synthesis of FePt Nanoparticles with Tunable Size, J. Am. Chem. Soc. 126 (2004) 8394–8395.

[26]. M. Chen, J. Kim, J.P. Liu, H. Fan, S. Sun, Synthesis of FePt Nanocubes and Their Oriented Self-Assembly, J. Am. Chem. Soc. 128 (2006) 7132–7133.

[27]. Q. Liu, Z. Yan, N.L. Henderson, J.C. Bauer, D.W. Goodman, J.D. Batteas, R.E. Schaak, Synthesis of CuPt Nanorod Catalysts with Tunable Lengths, J. Am. Chem. Soc. 131 (2009) 5720–5721

[28]. S. Mourdikoudis, L.M. Liz-Marzán, Oleylamine in Nanoparticle Synthesis, Chem. Mater. 25 (2013) 1465–1476.

[29]. M. Sarno, E. Ponticorvo, C. Cirillo, High surface area monodispersed Fe_3O_4 nanoparticles alone and on physical exfoliated graphite for improved supercapacitors, J. Phys. Chem. Solids 99 (2016) 138–147.

[30]. S.J. Rowley-Neale, D.A.C. Brownson, G.C. Smith, D.A. Sawtell, P.J. Kelly, C.E. Banks, 2D nanosheet molybdenum disulphide (MoS_2) modified electrodes explored towards the hydrogen evolution reaction, Nanoscale 7 (2015) 18152–18168.

[31]. K.D. Rasamani, F. Alimohammadi, Y. Sun, Interlayer-expanded MoS_2, Mater. Today 20 (2017) 83–91.

[32]. M.A. Shah, Growth of uniform nanoparticles of platinum by an economical approach at relatively low temperature, Sci. Iran. 19 (2012) 964–966.

[33]. C.P. Veeramalai, F. Li, Y. Liu, Z. Xu, T. Guo, T.W. Kim, Enhanced field emission properties of molybdenum disulphide few layer nanosheets synthesized by hydrothermal method, Appl. Surf. Sci. 389 (2016) 1017–1022.

[34]. M. Sarno, E. Ponticorvo, Effect of the amount of nickel sulphide, molybdenum disulphide and carbon nanosupport on a Tafel slope and overpotential optimization, Nanotechnology 28 (2017) 214003–214010.

[35]. M. Sarno, E. Ponticorvo, Much enhanced electrocatalysis of Pt/PtO_2 and low platinum loading Pt/PtO_2-Fe_3O_4 dumbbell nanoparticles, Int. J. Hydrog. Energy 42 (2017) 23631–23638.

[36]. N. Krstajic, S. Trasatti, Cathodic behaviour of RuO_2-doped Ni/Co_3O_4 electrodes in alkaline solutions: hydrogen evolution, J. Appl. Electrochem. 28 (1998) 1291–1297.

[37]. M.A. Domínguez-Crespo, E. Ramírez-Meneses, A.M. Torres-Huerta, V. Garibay-Febles, K. Philippot, Kinetics of hydrogen evolution reaction on stabilized Ni, Pt and Ni–Pt nanoparticles obtained by an organometallic approach, Int. J. Hydrog. Energy 37 (2012) 4798–4811.

[38]. X. Weng, Y. Liu, K.K. Wang, J.J. Feng, J. Yuan, A.J. Wang, Q.Q. Xu, Single-step aqueous synthesis of AuPt alloy nanodendrites with superior electrocatalytic activity for oxygen reduction and hydrogen evolution reaction, Int. J. Hydrog. Energy 41 (2016) 18193–18202.

[39]. Y. Li, H. Wang, L. Xie, Y. Liang, G. Hong, H. Dai, MoS_2 Nanoparticles Grown on Graphene: An Advanced Catalyst for Hydrogen Evolution Reaction, J. Am. Chem. Soc. 133 (2011) 7296–7299.

[40]. Q. Li, L. Wu, G. Wu, D. Su, H. Lv, S. Zhang, W. Zhu, A. Casimir, H. Zhu, A. Mendoza-Garcia, S. Sun, New Approach to Fully Ordered fct-FePt Nanoparticles for Much Enhanced Electrocatalysis in Acid, Nano Lett. 15 (2015) 2468−2473.

[41]. A. Zhang, S. Yu, Y. Jiang, L. Jia, X. Xia, W. Ye, C. Wang, A novel Pt@Te-reduced graphene oxide/polyimide composite catalyst for hydrogen evolution, Int. J. Hydrog. Energy 40 (2015) 16238–16247.

[42]. L.L. Zhu, H.P. Lin, Y.Y. Li, F. Liao, Y. Lifshitz, M. Sheng, S.T. Lee, M. Shao, A rhodium/silicon co-electrocatalyst design concept to surpass platinum hydrogen evolution activity at high overpotentials, Nat. Commun. 7 (2016) 12272, 1-7.

[43]. R.T.S. Oliveira, M.C. Santos, P.A.P. Nascente, L.O.S. Bulhões, E.C. Pereira, Nanogravimetric and Voltammetric Studies of a Pt-Rh alloy Surface and its Behavior for Methanol Oxidation, Int. J. Electrochem. Sci. 3 (2008) 970–979.

[44]. Z. Liu, Z.Y. Ling, X. Su, J.Y. Lee, Carbon-Supported Pt and PtRu Nanoparticles as Catalysts for a Direct Methanol Fuel Cell, J. Phys. Chem. B 108 (2004) 8234–8240.

[45]. G.H. An, E.H. Lee, H.J. Ahn, Ruthenium and ruthenium oxide nanofiber supports for enhanced activity of platinum electrocatalysts in the methanol oxidation reaction, Phys. Chem. Chem. Phys. 18 (2016) 14859–14866.

[46]. J.Y. Chen, Q.J. Niu, G.K. Chen, J. Nie, G.P. Ma, Electrooxidation of Methanol on Pt @Ni Bimetallic Catalyst Supported on Porous Carbon Nanofibers, J. Phys. Chem. C, 121 (2017) 1463–1471.

[47]. Z. Wang, C. Lu, W. Kong, Y. Zhang, J. Li, Platinum nanoparticles supported on core–shell nickel–carbon as catalyst for methanol oxidation reaction, J. Alloy. Comp. 690 (2017) 95–100.

[48]. Y.J. Gu, W.T. Wong, Nanostructure PtRu/MWNTs as Anode Catalysts Prepared in a Vacuum for Direct Methanol Oxidation, Langmuir 22 (2006) 11447–11452.

[49]. S.-S. Li, J. Yu, Y.-Y. Hu, A.-J. Wang, J.-R. Chen, J.-J. Feng, Simple synthesis of hollow Pt–Pd nanospheres supported on reduced graphene oxide for enhanced methanol electrooxidation, J. Power Sources 254 (2014) 119-125.